PHYSICAL REVIEW E VOLUME 56, NUMBER 2 AUGUST 1997

High-Reynolds-number thermal turbulence in mercury

A. Naert, T. Segawa, and M. Sano
Research Institute of Electrical Communication, Tohoku University, Sendai 980, Japan
(Received 4 March 1997)

We have studied the scaling properties of turbulence in a Rayleigh-Bénard convection cell, using a low-Prandtl-number (Pr) fluid, Hg (Pr=0.024). The length scales of thermal and viscous layers, analyzed from time series of movable thermistors near the cold upper plate, revealed that the viscous boundary layer is thinner than the thermal one over the observed range of Rayleigh numbers ($10^6<\mathrm{Ra}<10^8$). This feature, peculiar to low Pr fluid convection, differed from what is commonly observed in He, water, or other fluids. The scaling of Reynolds number Re and Nusselt number Nu has been investigated using different aspect ratio cells ($\Gamma=0.5,\ 1$, and 2) for a wider range of Ra. The hypothetical ultimate regime ($\mathrm{Nu}\sim\mathrm{Ra}^{1/2}$) was not observed in the range $10^5<\mathrm{Ra}<2\times10^9$ even though the two boundary layers are inverted. [S1063-651X(97)50708-2]

PACS number(s): 47.27.−i

Experimental studies on turbulent thermal convection have revealed a distinct state called hard turbulence [1–5]. This regime is characterized by the following features: (1) The histogram of the temperature fluctuations in the central region of the cell has an exponential-like shape. (2) Large scale stable bulk circulation coexists with turbulent fluctuations. (3) The Nusselt number Nu, the root mean square of the temperature fluctuation, and the mean velocity U of the large scale flow all have power law dependence on the Rayleigh number Ra, with scaling exponents different from those given by classical theory [6]. (4) The temperature power spectrum decays as a power law with a slope close to -1.4 for $\mathrm{Ra}<10^{11}$ and two slopes for $\mathrm{Ra}>10^{11}$.

Theories predicting scaling relations in hard turbulence assume distinct boundary layers for temperature and velocity (viscous sublayer) fields [2,6,7]. Provided that the thermal boundary layer is purely diffusive, and confined in the viscous one, the theory gives 2/7 for the Nusselt number scaling exponent (Nu: nondimensional heat flux) [2,7]. This value has been confirmed by experiments in helium gas [3]: 0.285 ± 0.004. Shraiman and Siggia [7] conjectured that hard turbulence is unstable if crossing of two boundary layers occurs. Therefore this state may not be asymptotic for high Ra, but intermediate. The relation, $\mathrm{Nu}\sim\mathrm{Ra}^{1/2}$, was predicted for this new state [6–8].

In recent experiments using pressurized SF_6, Belmonte *et al.* measured the dependence of the thermal and viscous boundary layer thickness, λ_T and λ_V, respectively, on Ra. The values of the two scaling exponents are such that, at high enough Rayleigh numbers, the viscous boundary layer may become thinner than the thermal one, violating the hypothesis that the thermal boundary layer is diffusion limited. This crossing was estimated to take place around $\mathrm{Ra}\sim10^{14}$, though these Ra were not obtained [9]. However, the lower the Prandtl number, the smaller the ratio of the boundary layer thicknesses, λ_V/λ_T, since the Reynolds number is higher for the same Ra. The Rayleigh number for this ''transition'' in Hg was recently evaluated to be of the order of 10^5 [10]. Therefore, the motivation to study thermal turbulence in low Pr fluid is clear: it allows one to investigate important regimes of turbulence at moderate values of Ra, which are otherwise difficult to realize in well controlled experimental conditions.

In this paper we examine the statistical and scaling properties of turbulence in Hg. We studied the thermal and viscous boundary layers, and Nusselt number scaling for Ra number up to 2×10^9. We compare our results to those obtained in helium and SF_6. The Reynolds number of the flow is about 20 times higher than that of He at the same Ra, in the same geometry [11]. The experimental cell is a vertical cylinder of 10 cm height (L) and 10 cm (D) in diameter as shown in Fig. 1. Most of experimental data were measured using this aspect ratio ($\Gamma\equiv D/L=1$). In order to cover a wider range of Ra, we used two other cells: 5 cm height ($\Gamma=2$) and 20 cm height ($\Gamma=1/2$). The top and bottom plates are made out of copper (2 cm thick), plated with nickel and chromium. The side wall cylinder is made of 2 mm thick stainless steel. Heating and cooling systems were described previously in [11]. The temperature of the top and bottom plates is given by thermistors embedded in holes. All the thermistors have been calibrated together with a standard one to an accuracy of 10^{-3} K. Because the thermistors are not located directly on the cell's surface, we had to evaluate the temperature drop in the copper to calculate precisely Ra. Our measurement of the temperature profile in the boundary layer (see below) allows one to evaluate the heat flux in mercury near the plate, on the axis of the cell. By continuity, this flux is the same as in the copper. It gives the temperature drop in the copper (about 3% of ΔT at 100 W, and 0.5% at 1 W). The convection cell is surrounded by a thermal insulator and placed in a stainless steel jacket with a copper bottom, whose temperature is set to the temperature of the bottom plate of the cell, with a second water circulation (see Fig. 1). The maximal heat leakage was tested and found to be less than 0.1 W at the highest temperature difference attained in this experiment. To measure the local temperature fluctuations, we used five thermistors (Thermometrics B07PA) whose size is 300 μm in diameter with insulation, though the bare size is 200 μm. Their response time is sufficiently shorter than the typical minimum time scale of flow; 100–200 ms. As shown in Fig. 1, one thermistor [A] is placed at the center of the cell at midheight, two are vertically aligned 1 cm from the side wall, one at midheight [$B1$], and the other 2 mm above [$B2$] to measure the mean flow velocity. Two thermistors ([C] and [D]) are fixed on a 0.8 mm diameter stainless steel

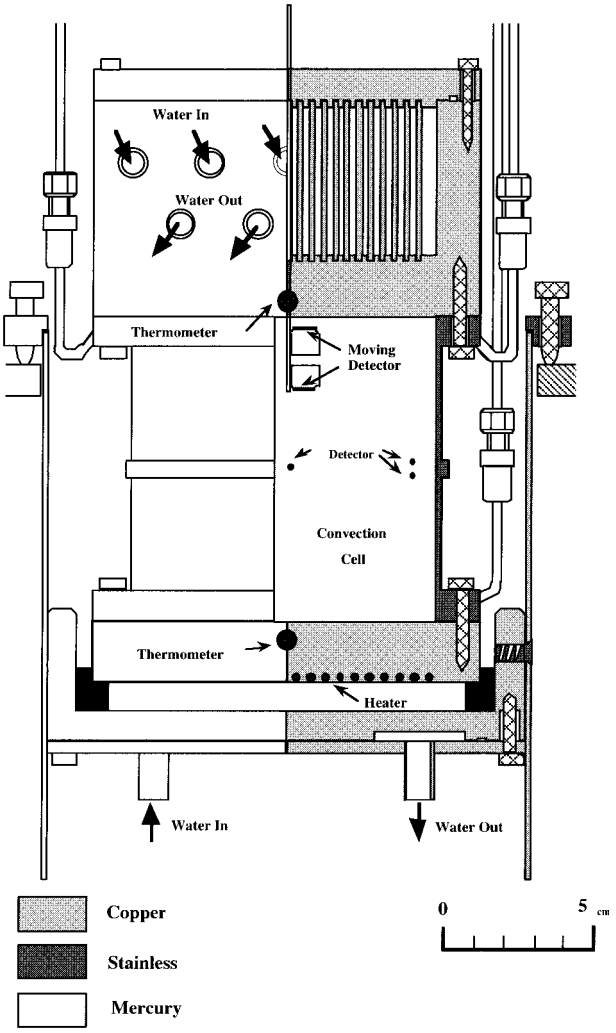

FIG. 1. Schematic drawing of the experimental cell with the positions of the thermistors.

tube, which is tied to a micro-translational stage, controlled by a stepper motor moving vertically along the center line of the cylinder. Each thermistor constitutes one arm of an ac capacitance bridge whose output is fed to a lock-in amplifier (PAR 124A). The output signal is first digitized and stored in a HP digital spectrum analyzer (HP3563A) and then analyzed by a computer.

We measured the thermal and viscous boundary layer directly, using the movable thermistors $[C]$ and $[D]$. For different locations of the thermistors, we record long samples of signal (122 000 points). Due to the low frequencies in mercury, a measurement takes from 4 to 13 h depending on the value of Ra. The data acquisition and the movement of the detector are automated. Figure 2 shows histograms of temperature fluctuations at various heights along the center line of the cylinder. When the thermistor is well within the two boundary layers, the probability density function is close to Gaussian. For larger distances, it becomes strongly asymmetric, and approaches an exponential-like distribution as the detector moves toward the center.

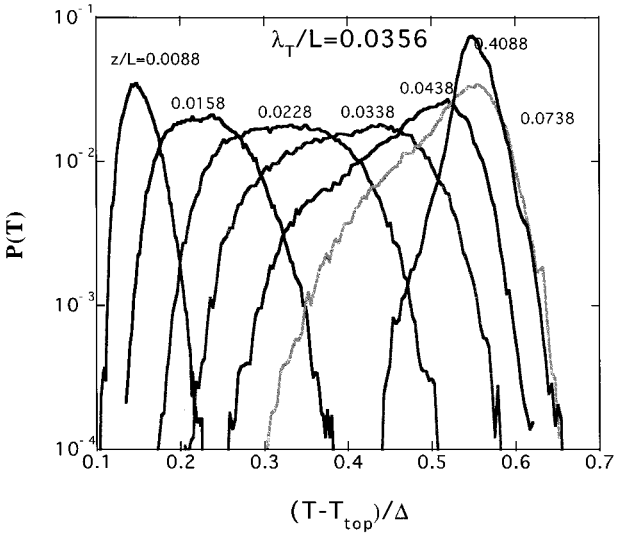

FIG. 2. Probability distribution function of temperature fluctuations at various heights, z/L, at Ra$=2.8\times10^7$.

Thermal boundary layer

From the temperature signal at different distances from the cold plate and different Ra, we compute the mean value and the rms [see Fig. 3(a)]. To obtain a characteristic thermal length from this profile, the boundary layer thickness λ_T, we used three independent methods that coincide nicely. The first one is to draw $\langle T(z)\rangle$ at a small distance from the plate. λ_T is then defined as the distance where this tangent intersects the saturated value of $\langle T(z)\rangle$ as $z\rightarrow L/2$. The second method is to evaluate the distance z where the rms of the fluctuation is the maximum. This is done by a parabolic fitting of the rms in the vincinity of its maximum. The last method is to fit the profile of $\langle T(z)\rangle$ with a convenient function of the nondimensional variable: z/λ_T. We used a hyperbolic tangent. The resulting values of λ_T for different Ra are plotted in Fig. 4 together with the velocity boundary layer thickness to be discussed below. We show in the same figure the best fit of λ_T ($\propto \mathrm{Ra}^{-0.2\pm0.02}$), and for comparison, a power law of exponent -0.25. This latter law is the inverse of the Nusselt number scaling, which is expected if the heat transfer through the boundary layer is governed by diffusion. One can note in Fig. 3(a) that the value of the mean temperature out of the upper plate boundary layer is larger than the value $T/2$ in the center of the cell, revealing a slight temperature inversion in the cell ($\simeq 10\%$ of the total temperature difference ΔT). Out of the boundary layer regions, the flow comes under a stable stratification in temperature. The amplitude of the temperature fluctuations is about 3% of ΔT, which is significantly smaller than the temperature inversion.

Viscous boundary layer

Because of the high thermal conductivity of mercury and the large fluctuations of temperature in convective flows, a direct measurement of the velocity is so far out of reach. To investigate the velocity boundary layer, we used an indirect method based on the temperature fluctuations signal [9,11]. It relies on the assumption that the highest frequency of the

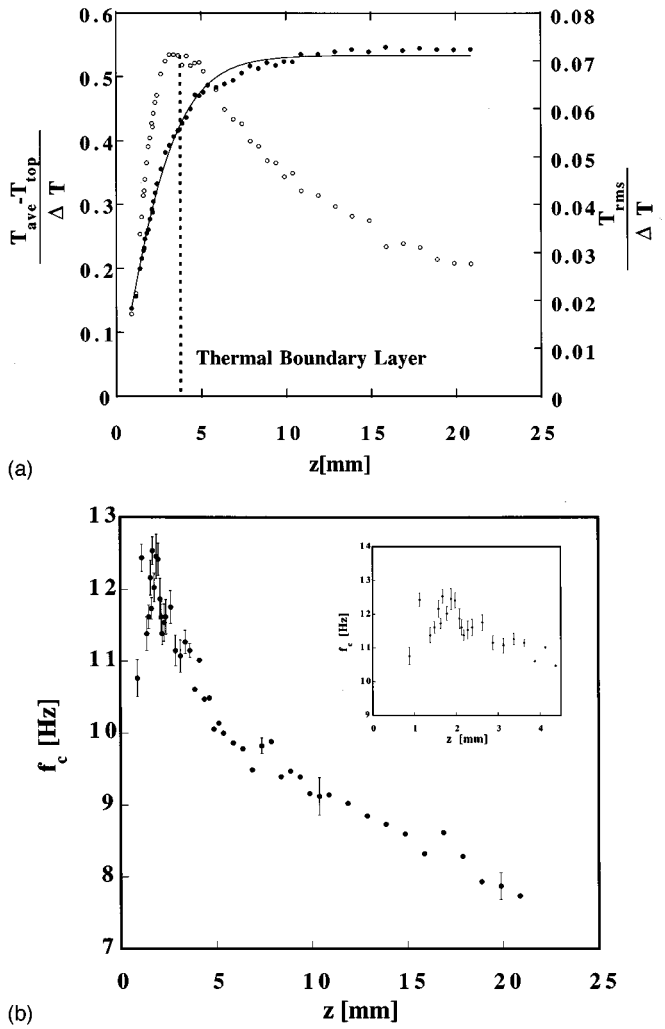

FIG. 3. (a) Temperature profile (●) and root-mean-square fluctuations (○) near the top plate, measured by the movable thermistor $[C]$, at Ra$=6.1\times10^7$. The solid line is the best fit to the function, $T_{\rm ave}(z)-T_{\rm top}=m_1\tanh(m_2 z)$. The guide line shows the thermal boundary layer thickness. (b) The profile of the frequency f_c as a function of the distance z from the top plate, at Ra$=6.1\times10^7$. The distance at which f_c reaches its maximum approximates the viscous boundary layer thickness.

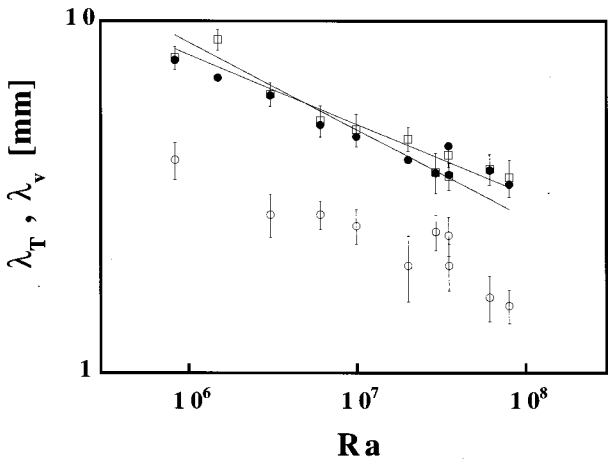

FIG. 4. Thickness of the thermal and viscous boundary layers as a function of Ra. Thermal boundary layer length is determined by the fitting the average temperature profile (●), and by the position of the maximum rms fluctuations (□). The best fit gives: $\lambda_T \propto {\rm Ra}^{-0.2\pm0.02}$. We plotted for comparison a power law of exponent -0.25, inverse of the Nu's scaling. Viscous sublayer length is determined from the position of the maximum cutoff frequency f_c of the power spectrum (○).

temperature fluctuation is due to the advection of the smallest ''thermal structures,'' of size l: $f_c\sim\langle v\rangle/l$, l being constant, in the range of interest: $z<\lambda_T$. The validity of this method has only been tested in a water experiment where velocity could also be measured by particle tracing [9]. In that case (Pr$=6$), the size l is identified to the size of the plumes, roughly the thermal boundary layer thickness λ_T. In Hg, the boundary layers are qualitatively different, and the existence of plumes is even questionable. However, the size of the smallest thermal structure cannot change much on a distance of the order of the boundary layer thickness λ_T. This justifies the formula $f_c\sim\langle v\rangle/l$, whatever the length l may represent. The only assumption done here is that the maximum of $\langle v\rangle$ occurs at the same distance from the plate as the maximum of f_c. We call this distance λ_v: the viscous boundary layer thickness. As in [9] we define the highest frequency as the intersection between the power spectrum and the white background noise, which has roughly a constant level. A typical profile of f_c is plotted in Fig. 3(b). We checked that, using a reference level ten times higher than the background noise, or an arbitrary reference level (-70 dB), gives a similar profile, with slightly lower frequencies. The maximum is at the same position λ_v. The result for λ_v is therefore independent of the method used to measure the frequency. The boundary layer thickness λ_v is plotted for several values of Ra in Fig. 4. The dispersion of λ_v is mainly a consequence of the indistinctness of the maximum frequency f_c. Even though it is difficult at this point to establish the scaling of λ_v versus Ra, it is clear that in Hg, $\lambda_v<\lambda_T$ over the observed range of Ra ($10^6<{\rm Ra}<10^8$).

A low frequency oscillation of the temperature has been observed in several Rayleigh-Bénard experiments using different fluids [2,3,11]. This frequency f_p is clearly identified as a peak on the power spectrum of the temperature. The mean velocity of the flow has been measured previously [11] from the cross correlation of the signal given by two thermistors $[B1]$ and $[B2]$ located along the side wall of the cell. The Reynolds number calculated with the diameter L of the cell and this velocity has been found to coincide with the one obtained through the low frequency peak [3,11]: ${\rm Re}=4f_pL^2/\nu$. In the present work, we investigated the scaling of f_p versus Ra in two cells of aspect ratio 1 and 2. In our larger cell, of aspect ratio 1/2, we noted that the peak is absent from the power spectrum. The frequency f_p is plotted in Fig. 5 as a function of Ra. The two curves corresponding to the two different aspect ratio cells show similar scaling relations: $f_p\propto{\rm Ra}^{0.44\pm0.02}$ and $f_p\propto{\rm Ra}^{0.4\pm0.04}$, respectively, in cells of aspect ratio 1 and 2 for Ra higher than 10^5. The exponent is consistent with our previous result (0.46 ± 0.02 in [11]) and the value 0.424 obtained recently by Cioni *et al.* [10] in their mercury aspect ratio 1 cell. However, it is slightly smaller than the value 0.48 usually obtained in higher Pr fluid experiments.

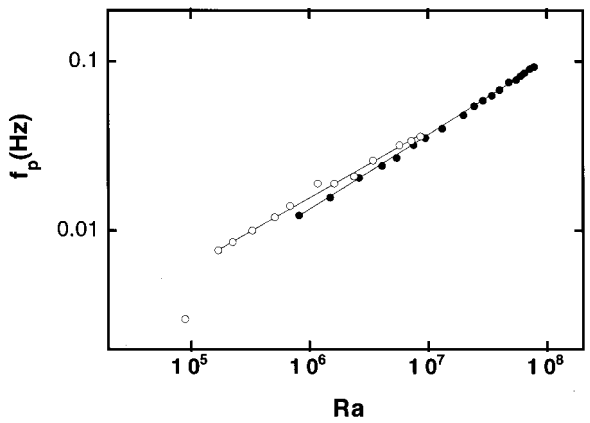

FIG. 5. Scaling of low frequency peak vs Ra. The two symbols: ● and ○ refer to the aspect ratio 1 and 2 cells, respectively. The best fit gives $f_p \propto \mathrm{Ra}^{0.44\pm0.02}$ in the aspect ratio 1 cell, and $f_p \propto \mathrm{Ra}^{0.4\pm0.04}$ in the aspect ratio 2 cell, for Ra higher than 10^5.

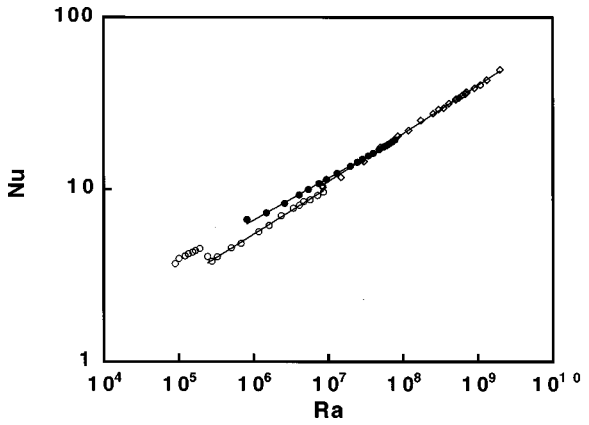

FIG. 6. Scaling of Nusselt number as a function of Ra. The symbols ●, ○, and ◇, refer to the aspect ratio 1, 2, and 1/2 cells, respectively. For the $\Gamma=1$ cell, the scaling exponents are 0.25 ±0.005, for the $\Gamma=1$ cell, 0.28 ± 0.02 for $\Gamma=0.5$ cell, and 0.27 ±0.02 for $\Gamma=2$ cell.

Since the inversion of the two boundary layers was observed, we investigated the hypothetical ultimate high Ra regime of Nusselt scaling, $\mathrm{Nu}\sim\mathrm{Ra}^{1/2}$, using three different cells. The three cells have the same diameter (10 cm), as the heights are 5, 10, and 20 cm for the aspect ratios $\Gamma=0.5$, 1, and 2, respectively. Each cell covers the range of Ra, $10^5<\mathrm{Ra}<10^7$, $10^6<\mathrm{Ra}<10^8$, and $10^7<\mathrm{Ra}<2\times10^9$, respectively. For the $\Gamma=2$ cell, one can see in Fig. 6 that the Nu curve has a bump around $\mathrm{Ra}\sim2\times10^5$. For higher Ra, the histogram of the temperature fluctuation at the center of the cell has one maximum, but two for the smaller values of Ra. This may indicate a transition in the flow configuration, from two to one single roll, for increasing Ra. Above this value, the Nu curve shows a well defined scaling law, with the exponent 0.27 ± 0.02. For the $\Gamma=1$ cell, the scaling exponent for Nu is 0.25 ± 0.005, consistent with our previous value 0.27 ± 0.02 [11], and the result of Cioni *et al.* 0.26 ± 0.02 [10]. For $\Gamma=0.5$ cell, the scaling exponent is 0.28 ± 0.02. The highest Ra number, $\mathrm{Ra}=2\times10^9$, was attained in this cell, at a heating power about 1 kW, with $\Delta T\sim100$ K. No significant change in heat flux characteristic was observed, which is different from the recent result of Cioni *et al.* [10]. Although, with the same experimental procedure, three different aspect ratio cells give a slight shift in Nu, the scaling exponents are almost the same.

$\mathrm{Nu}\sim\mathrm{Ra}^{1/2}$ was not observed even though the two boundary layers are inverted. Explaining the thermal turbulent state with inverted boundary layers is a challenge for scaling theory of thermal turbulence.

We are grateful to M. Sugawara for building the experimental cell and to J. A. Glazier, Y. Sawada, S. Toh, X. Z. Wu, A. Belmonte, S. Cioni, and S. Ciliberto for stimulating discussions. This work was supported by Japanese Grant-in-Aid for Science Research Fund from the Ministry of Education, Science and Culture (No. 08454104, 09440146). A.N. acknowledges support from the EC/JSPS1 (European Community and Japanese Society for the Promotion of Science), and for the warm hospitality of Tohoku University.

[1] F. Heslot, B. Castaing, and A. Libchaber, Phys. Rev. A **36**, 5870 (1987).
[2] B. Castaing *et al.*, J. Fluid Mech. **204**, 1 (1989).
[3] M. Sano, X.Z. Wu, and A. Libchaber, Phys. Rev. A **40**, 6421 (1989); X.Z. Wu and A. Libchaber, *ibid.* **45**, 842 (1992).
[4] X.Z. Wu, L.P. Kadanoff, A. Libchaber, and M. Sano, Phys. Rev. Lett. **64**, 2140 (1990).
[5] T.H. Solomon and J. P. Gollub, Phys. Rev. Lett. **64**, 2382 (1990); Phys. Rev. A **43**, 6683 (1991).
[6] W.V.R. Malkus, Proc. R. Soc. London, Ser. A **225**, 185 (1954); L. N. Howard, J. Fluid Mech. **17**, 405 (1963).
[7] B.I. Shraiman and E.D. Siggia, Phys. Rev. A **42**, 3650 (1990).
[8] R. Kraichnan, Phys. Fluids **5**, 1374 (1962).
[9] A. Belmonte, A. Tilgner, and A. Libchaber, Phys. Rev. Lett. **47**, 4067 (1993); Phys. Rev. E **50**, 269 (1994).
[10] S. Cioni, S. Ciliberto, and J. Sommeria, J. Fluid Mech. **335**, 11 (1997).
[11] T. Takeshita, T. Segawa, J.A. Glazier, and M. Sano, Phys. Rev. Lett. **76**, 1465 (1996).